



Article

Reapplication Potential of Historic Pb–Zn Slag with Regard to Zero Waste Principles

Dragan Radulović¹, Anja Terzić^{2,*}, Jovica Stojanović¹, Vladimir Jovanović¹, Dejan Todorović¹ and Branislav Ivošević¹

¹ Institute for Technology of Nuclear and Other Mineral Raw Materials, Franchet d'Esperey 86, 11000 Belgrade, Serbia; d.radulovic@itnms.ac.rs (D.R.); j.stojanovic@itnms.ac.rs (J.S.); v.jovanovic@itnms.ac.rs (V.J.); d.todorovic@itnms.ac.rs (D.T.); b.ivošević@itnms.ac.rs (B.I.)

² Institute for Materials Testing—IMS, Bulevar Vojvode Mišića 43, 11000 Belgrade, Serbia

* Correspondence: anja.terzic@institutims.rs

Abstract: Smelting used to be less efficient; therefore, wastes obtained from historical processing at smelter plants usually contain certain quantities of valuable metals. Upon the extraction of useful metal elements, metallurgical slag can be repurposed as an alternative mineral raw material in the building sector. A case study was conducted, which included an investigation of the physico-chemical, mineralogical, and microstructural properties of Pb–Zn slag found at the historic landfill near the Topilnica Veles smelter in North Macedonia. The slag was sampled using drill holes. The mineralogical and microstructural analysis revealed that Pb–Zn slag is a very complex and inhomogeneous alternative raw material with utilizable levels of metals, specifically Pb (2.3 wt.%), Zn (7.1 wt.%), and Ag (27.5 ppm). Crystalline mineral phases of wurtzite, sphalerite, galena, cerussite, akermanite, wüstite, monticellite, franklinite, and zincite were identified in the analyzed samples. The slag's matrix consisted of alumino-silicates, amorphous silicates, and mixtures of spinel and silicates. Due to the economic potential of Pb, Zn, and Ag extraction, the first stage of reutilization will be to transform metal concentrates into their collective concentrate, from which the maximum amount of these crucial components can be extracted. This procedure will include combination of gravity concentration and separation techniques. The next step is to assess the Pb–Zn slag's potential applications in civil engineering, based on its mineralogical and physico-mechanical properties. Alumino-silicates present in Pb–Zn slag, which contain high concentrations of SiO₂, Al₂O₃, CaO, and Fe₂O₃, are suitable for use in cementitious building composites. The goal of this research is to suggest a solution by which to close the circle of slag's reutilization in terms of zero waste principles. It is therefore critical to thoroughly investigate the material, the established methods and preparation processes, and the ways of concentrating useful components into commercial products.

Keywords: critical raw materials; alternative deposits; secondary resources; building materials; instrumental analyses; microscopy



Citation: Radulović, D.; Terzić, A.; Stojanović, J.; Jovanović, V.; Todorović, D.; Ivošević, B. Reapplication Potential of Historic Pb–Zn Slag with Regard to Zero Waste Principles. *Sustainability* **2024**, *16*, 720. <https://doi.org/10.3390/su16020720>

Academic Editor: Rajesh Kumar Jyothi

Received: 21 December 2023

Revised: 11 January 2024

Accepted: 12 January 2024

Published: 14 January 2024



Copyright: © 2024 by the authors. Licensee MDPI, Basel, Switzerland. This article is an open access article distributed under the terms and conditions of the Creative Commons Attribution (CC BY) license (<https://creativecommons.org/licenses/by/4.0/>).

1. Introduction

After copper and aluminum, zinc and lead are two non-ferrous metals prevalently utilized in various industrial branches [1]. In 2022, the amount of zinc mined worldwide was 13 million tons [2,3]. According to the GHG Protocol Standard's methodology, the carbon footprint of zinc production is approximately 0.93 tons CO₂e per ton of zinc [4]. Zinc is commonly used in the galvanizing process, which keeps steel and iron from rusting. In 2022, a total of 4.49 million metric tons of lead were mined worldwide [2]. Lead is used in a variety of applications, including radiation shielding, fusible alloys, lead–acid batteries, and construction materials [5]. Lead has a smaller carbon footprint than zinc, ranging from 0.30 to 0.76 tons CO₂e per ton of Pb [6]. Lead and zinc are typically obtained as byproducts of metal mining and smelting [7]. Due to ecological issues, hydrometallurgical

methods currently account for the vast majority of the world's production of both of these metals; however, pyrometallurgical processing still accounts for 10% to 20% of Zn and Pb output [8]. Smelter slags are a source of 70 kt/y and 7 kt/y of Zn and Pb, respectively. Both zinc and lead are found mainly in amorphous phases but also as ZnO, ZnS, Pb apatite, and PbSO₄ [1]. As a result, it is expected that there are certain quantities of reusable Zn and Pb in the metallurgical slag.

One large problem is that, due to a lack of economically viable technology, the vast majority of metallurgical waste materials are disposed of or are temporarily stored in non-hazardous industrial solids storage facilities or in open landfills. Slag from metallurgical processes is a significant source of pollutants, such as heavy metals and sulfide minerals, which are extremely hazardous to human health as well as to aquatic and soil environments, even when standard control measures have been implemented [9–11]. Current methods of treating metallurgical slags, such as reprocessing, desulfurization, backfilling, and restoration, are not widely used due to their high cost and/or low efficiency [12]. Waste materials placed near closed mining sites or smelters in isolated rural areas, in particular, have received much less attention because the local government cannot afford the high costs associated with managing and disposing of the waste in an environmentally responsible manner [13,14]. This is one of the main reasons that the reapplication of the Pb–Zn historic slag from rural areas was assessed in this study. The other reason is to contribute to the development of globally accepted waste treatment solutions that are economically, environmentally, and technically feasible.

One of the main contemporary guidelines is to reuse and recycle slag in fields, such as the building materials industry and civil engineering, that are the largest users of mineral raw materials and natural resources. Prior to repurposing Pb–Zn slag in the construction sector, it is important to analyze its mineralogical composition for the extraction of critical metals with economic potential, such as Pb, Zn, and Ag. As a result, procedures, such as gravity concentration and separation techniques, are being used to convert metal concentrations into a collective concentrate from which the maximum amount of one or more elements can be extracted [15,16]. Once valuable metal elements are extracted from the slag, the residual raw material has to be reapplied in order to close the cradle-to-cradle circle and achieve the zero-waste goal.

The production of construction materials could be a viable way by which to sustainably utilize Pb–Zn slag (upon extraction of valuable metal elements) with a financial return, given the slag's quantity and mineralogical composition, especially if the final products could be manufactured and sold locally [17]. This coincides with the 17 sustainable development goals (SDGs) proposed by the United Nations to advance social and environmental justice under the 2030 Agenda for Sustainable Development [18,19]. The 2030 Agenda emphasizes the need for sustainable management of the environment and its resources. Various sectors, such as mining, metallurgy and civil engineering, are under pressure to create sustainable technologies in order to meet the relevant SDGs.

The application of a recycled material in the building industry can be demanding if all sides of the problem are to be taken into account. These include proper application for the secondary raw material, economic viability of the final product, and its environmental impact. This is, however, not impossible, because various methods for the reapplication of different metallurgical slags have thus far been proposed. These include mortar, concrete, geopolymer, alkali-activated material, and traditional building ceramics. The idea is to cut down on energy use and carbon emissions by producing environmentally friendly and sustainable building materials in which a major component is replaced by metallurgical slag. The majority of the studies have demonstrated that building materials based on metallurgical slags show good performance. For example, from the standpoint of mechanical properties, Pb–Zn slag could replace up to 50% of the raw materials in mortar and concrete mixes. Lead–zinc slag can increase the physico-mechanical and durability properties of concrete and mortar, even at higher replacement rates [20–23]. It can also increase the durability of self-compacting concrete by up to 25%. One important problem brought on by the disposal

of lead–zinc slag is leaching, which can be effectively controlled by immobilization of the slag in mortar, concrete, geopolymer, and alkali-activated material [20]. Metallurgical slags are successfully repurposed as raw materials for making sintered, autoclaved, and unfired (adobe) bricks [12,24–26]. Additionally, high-value glass ceramic using lead slag and lead–zinc tailings is being successfully produced [27]. In line with the expanding trend of waste reutilization and clean manufacturing, geopolymers have been synthesized to immobilize Pb^{2+} and Zn^{2+} by simultaneously using electrolytic manganese residue and lead–zinc smelting slag as raw aluminosilicate material (precursor) [28]. If the slags are similar to sand in terms of their granulometry, they may be utilized as fine aggregate in concrete [29]. Pb–Zn slags can also be used as a pozzolanic additive, as structural fill material in road construction and embankments, or as a base material for making bricks and tiles after undergoing the required processing, such as grinding [30–33]. Arsenic from wastewater from copper smelting has been successfully removed using zinc slag, allowing the wastewater's safe discharge [34]. Alkali-activated materials made by combining alkali solutions with solid precursors, such as metakaolin, slag, and fly ash, have shown excellent mechanical performance and extremely minimized leaching of heavy metals [35,36]. Thus, the possibilities for the application of Pb–Zn slags in construction are numerous.

In this light, one issue that has not been thoroughly examined up to this point is the reapplication of Pb–Zn slag as coarse aggregate in the design of cementitious building composites upon extraction of valuable metal elements from the slag. Additionally, finding a replacement for coarse aggregates is important because the building industry requires a large amount of natural resources to produce high-quality concrete due to increasing global urbanization. Natural aggregates, both fine and coarse, normally make up three-fourths of the concrete volume. As a result, Pb–Zn slag may be an answer to the pursuit of alternative waste materials that could be used as aggregate substitutes in concrete manufacturing. The final goal is to lower the cost of concrete manufacturing, the amount of energy used, and the amount of CO_2 emitted. As a result of the application of waste materials, landfill space is freed and repurposed, and the problem of natural resource depletion is alleviated. Reusing Pb–Zn slag after the extraction of valuable metals such as Pb, Zn, and Ag makes it possible to achieve a number of sustainable development goals (SDGs), including promoting life on land (SDG 15); ensuring that everyone has access to clean water and sanitation (SDG 6); promoting industry, innovation, and infrastructure (Goal 9); promoting responsible consumption and production (SDG 12); and combating climate change (SDG 13). In this regard, using Pb–Zn slag from smelter plants may represent one of the most promising possibilities for waste consumption and its reapplication in civil engineering.

In this study, the detailed characterization of historic Pb–Zn slag from the smelter Topilnica Veles has been conducted in order to assess both the possibility of extracting the valuable metals and of reusing the slag as an alternative raw material in the building industry.

2. Materials and Methods

The technogenic mineral raw material (Pb–Zn slag) from the Topilnica Veles smelter, North Macedonia (KEPS MONT GROUP Skopje, North Macedonia) was investigated. There are currently 2,000,000 t of this historic Pb–Zn slag located at the landfill near the smelter (Figures 1 and 2).

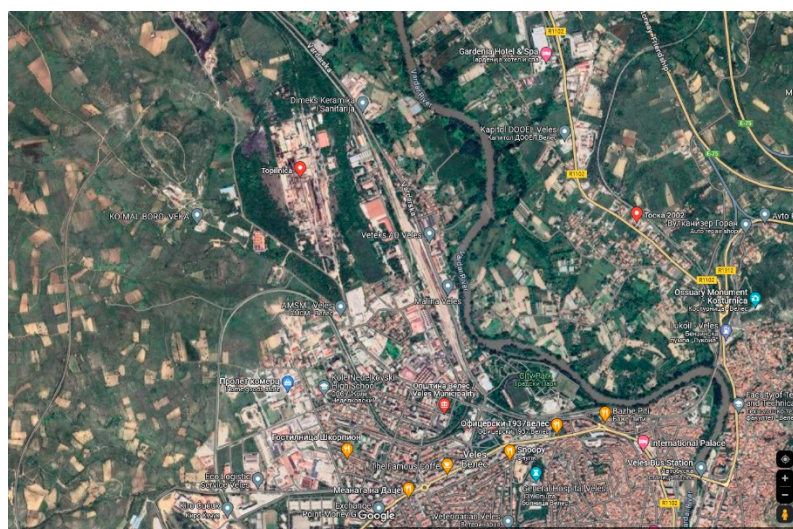


Figure 1. Proximity of the nearest urban settlement from the smelter and landfill (source: Google Maps).



Figure 2. Disposition of the open-air landfill near smelter plant (source: Google Maps).

The Pb–Zn slag was physico-chemically and mineralogically characterized in order to define the possibility of the valorization of useful metals and, subsequently, to assess the slag’s reapplication potential in the civil engineering industry. Figure 3 depicts the scheme of the employed experimental design regarding the possibility of the valorization of useful metals. Once the relevant properties of the studied alternative mineral raw material have been determined by the applied methodologies and instrumental techniques, all of the required parameters can be defined as a basis for additional technical tests (regarding the possibility of using Pb–Zn slag in cementitious building composites). Thereby, selecting the optimal process for valorizing Pb–Zn slag from Topilnica Veles allows the development of unique technological solutions for the extraction of valuable elements and the design of novel eco-friendly commercial building products.

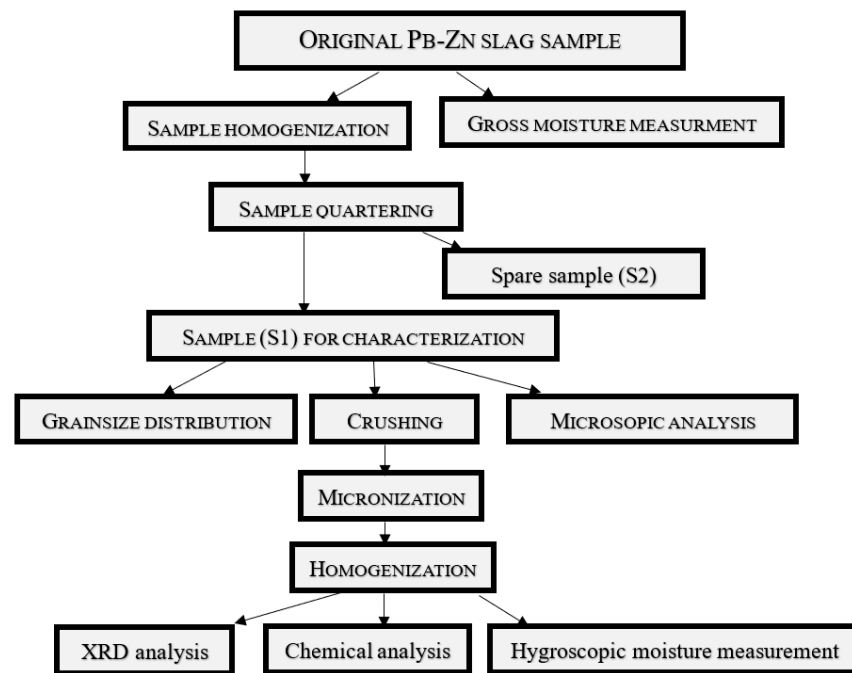


Figure 3. Scheme of the experimental design for characterization of Pb–Zn slag.

2.1. Sampling and Laboratory Processing of Pb–Zn Slag

The entire characterization was conducted on a representative sample of 50 kg of Pb–Zn slag obtained directly from the landfill (Figure 2). The mean grain diameter of the initial representative sample was 5.0 ± 0.00 mm. The procedure was conducted as described in Figure 3.

A share of the material was taken from the initial Pb–Zn slag sample in order to calculate the gross moisture content. The initial slag sample was then homogenized. Following homogenization, the obtained material was split into two samples (S1 and S2) using the quartering method. The S2 sample was stored, and the other half, i.e., the S1 sample, was used for further characterization as follows: (1) The grain-size distribution was determined using 5 kg of the original sample by means of Tyler’s standard series of sieves. In order to obtain very precise sieve analysis as well as the accuracy of the obtained results, the extraction of the sample material was conveyed with the utmost care. The optimum sampling method is one that yields the most representative sample from the product and meets the product’s required parameters. (2) The second part of this sample was used in a microscopic analysis to assess the presence of potentially useful minerals contained in the slag. The analysis was conducted on a representative sample (quartering approach). We ensured that the microscope was properly calibrated and that the objective lens was focused correctly. Measuring equipment specifically built for use with a microscope was employed to achieve reliable measurements. The photos were taken at the highest resolution available. A good light source was used to illuminate the specimen and to produce clear and sharp photos. The same specimen was recorded multiple times. (3) The third part of the sample underwent crushing (jaw and roll crushers) and micronization (using a planetary ball mill) to a mean particle size that was adequate for X-ray diffraction analysis, chemical analysis, and/or further physico-chemical characterization. Each test and analysis employed a representative sample (quartering approach).

2.2. Physical Characterization of the Pb–Zn Slag

The original Pb–Zn slag sample was removed from the sacks in which it was distributed to the laboratory and measured for gross moisture using the standard method. The

gross moisture content (M_g) was calculated on three initial samples of Pb–Zn slag, initially dried at room temperature (20 ± 2 °C) for 24 h, using the following equation (Equation (1)):

$$M_g = \frac{(m_{os} - m_{ads})}{m_{os}}, (\%) \quad (1)$$

where m_{os} is the mass of the original slag sample (g) and m_{ads} is the mass of the slag sample dried at ambient temperature (g).

The calculated value is the arithmetic mean of the measured values for each of the three samples. The initial samples of Pb–Zn slag had a gross moisture content of 0.9%.

The hygroscopic moisture content (M_h) was calculated as the mean of three measurements using Equation (2):

$$M_h = \frac{(m_s - m_{ds})}{m_s}, (\%) \quad (2)$$

where m_s is the mass of the slag sample upon crushing (g), and m_{ds} is the mass of the slag sample dried at 105 °C (g).

Pb–Zn slag had a hygroscopic moisture content of 0.11%.

Both gross and hygroscopic moisture content values are within acceptable limits for use in concrete, as most fine aggregates have a maximum drained moisture content of about 3% to 8%, whereas coarse aggregates have a maximum drained moisture content of about 1% to 6%.

2.3. Grain Size Distribution Analysis of Pb–Zn Slag

The grain size distribution was analyzed on the starting sample of Pb–Zn slag (mean grain size: $-5.0 + 0.00$ mm). The initial sample of Pb–Zn slag's granulometric composition was determined by sieving on Tyler's series of sieves (<https://wstyler.com/particle-analysis/test-sieves/wstyler-test-sieves/>, accessed on 21 December 2023), with the last sieve in the opening sequence being 0.1 mm.

2.4. Instrumental Analysis of Pb–Zn Slag

Chemical analysis, i.e., identification and quantification, of major oxides was conducted using the atomic absorption spectroscopy (AAS) technique on a PinAAcle 900 Perkin Elmer instrument (PerkinElmer, Waltham, MA, USA). AAS has a high degree of accuracy, with results typically ranging from 0.5 to 5%. It is a highly sensitive test procedure that can measure as low as parts per billion (g/kg) depending on the material under test. The instrument is a flame-only device with a real double-beam design for quick startup and long-term reliability. It has fiber optics to maximize light flow for greater detection limits, an eight-lamp mount, and automated flame and burner assembly optimization for increased production. Minor elements were detected via EDXRF analysis on a Spectro Xepos system (SPECTRO Analytical Instruments, Chelmsford, MA, USA) equipped with a 50 W and 60 V X-ray tube with a binary Co/Pd alloy thick target anode. The excitation mode of the X-ray tube was combined with polarized/direct excitation. The characteristic radiation emitted by the elements present in the sample was detected by a silicon drift detector with Peltier cooler system. Pulverized slag samples ($d_{50} < 63$ μm) were used in the analyses. Pb–Zn slag samples were dried at 105 °C prior to pulverization in a planetary ball mill.

X-ray diffraction (XRD) technique was applied to pulverized slag samples. XRD analysis enabled the determination of Pb–Zn slag's mineral composition. A Philips X-ray diffractometer, model PW-1710 (Philips Research, Eindhoven, The Netherlands), equipped with a scintillation counter and a curved graphite monochromator, was used to analyze the sample. The intensities of the diffracted $\text{CuK}\alpha$ X-ray radiation ($\lambda = 1.54178$ Å) were measured at room temperature in intervals of $0.02^\circ 2\theta$ and 1 s in the range from 4 to $65^\circ 2\theta$. The X-ray tube was loaded with a voltage of 40 kV and a current of 30 mA, while the slits for directing the primary and diffracted beams were each 1° and 0.1 mm.

The original (initial) Pb–Zn samples were used for optical microscopy. Medium-sized grain classes (approximately $-2.38 + 0.00$ mm) of the Pb–Zn slag were inserted in Plexiglas ‘plates’ for optical microscopy recording. The preparation area was 2.2 cm^2 . The originality of the starting grain mix was maintained by the quartering method. Visual examination of the samples helped to enable the diversity of mineral phases characteristic of the original slag sample. Carl Zeiss-Jena’s JENAPOL-U polarizing microscope for transmitted and reflected light (ZEISS, Reutlingen, Germany) was used for the analysis, along with a measuring tool. An Axiocam 105 color camera and the software package Carl Zeiss AxioVision SE64 Rel. 4.9.1 with the multiphase module were employed for the recording of the samples.

Scanning electron microscopy (SEM) was conducted on the micronized Pb–Zn samples. The testing sample was coated with carbon (20 nm layer, density 2.25 g/cm^3). The analysis was conducted on an SEM instrument, the JEOL JSM-6610LV (JEOL, Akishima, Tokyo, Japan) The magnification of this device is 5 to 300,000 times. The electron source was W wire, LaB 6. The voltage was 0.3–30 kV. The instrument works with a vacuum system: a rotary pump and turbomolecular pump (included in the basic configuration of the microscope), an ion pump (used for LaB6), and a rotary pump for working in low vacuum (10–270 Pa). For the detectors, we used an SE detector, BSE detector, CL detector, and EDS detector (model: X-Max Large Area Analytical Silicon Drift connected with INCAEnergy 350 Microanalysis System). For the detection of elements $Z \geq 5$; detection limit $\sim 0.1\text{ wt.}\%$, resolution 126 eV. Characteristics of the sample chamber: sample movement, 5-axis (X, Y, Z, T-tilt, R-rotation); maximum sample size, 20 cm (width), 8 cm (height), 1 kg (weight). Two infrared cameras were included. Standards used for microanalysis: 64 natural minerals and synthetic compounds. The device for coating samples with gold (Au) or carbon (C) is a LEICA SCD005 (Leica Microsystems, Wetzlar, Germany). Accompanying equipment included an ultrasonic bath, binoculars, etc. A voltage of 20 kV and an extinction time of 50 s were used. The lower limit of EDX sensitivity was $\sim 0.3\%$.

3. Results and Discussion

The input and output weights of sieves (M) were measured during the sieve analysis (described in Section 2.3). The acquired results are presented in Table 1. A diagram of the grain-size distribution for the initial Pb–Zn slag sample is provided in Figure 4.

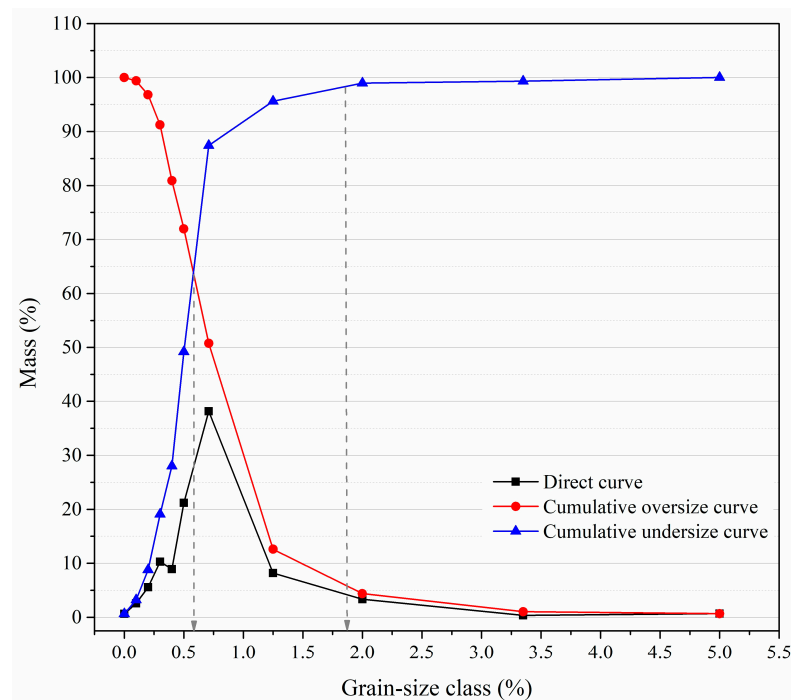


Figure 4. Grain-size distribution of the original Pb–Zn slag sample.

Table 1. Grain-size distribution of the original Pb–Zn slag sample.

Size Class (mm)	M (%)	↓ Σ M (%)	↑ Σ M (%)
+ 5.00	0.68	0.68	100.00
−5.00 + 3.35	0.35	1.03	99.32
−3.35 + 2.00	3.36	4.39	98.97
−2.00 + 1.25	8.21	12.60	95.61
−1.25 + 0.71	38.18	50.78	87.40
−0.71 + 0.50	21.20	71.98	49.22
−0.50 + 0.40	8.92	80.90	28.02
−0.40 + 0.30	10.31	91.21	19.10
−0.30 + 0.20	5.58	96.79	8.79
−0.20 + 0.10	2.59	99.38	3.21
−0.10 + 0.00	0.62	100.00	0.62
Input	100.00		

The average grain diameter (d50) and d80 parameter (particular screen size at which 80% of particles in the feed stream pass through) are 0.69 mm and 1.77 mm, respectively, as shown in Figure 4. The obtained grain-size distribution with certain modifications (addition of either natural or recycled concrete aggregate) can be considered suitable for concrete mix design.

Chemical analysis was conducted in order to determine whether the initial Pb–Zn slag sample contains useful metals, such as Pb and Zn, as well as precious metals, such as Ag. Additionally, the quantification of major oxides should indicate whether this waste material can be utilized as an alternative resource for the production of building materials such as cement clinker, mineral additive for bonding agents, and filler or aggregate for mortar and concrete. Table 2 shows the results from chemical composition identification using the methods described in Section 2.4.

Table 2. Chemical analysis of Pb–Zn slag.

Oxide	SiO ₂	Al ₂ O ₃	CaO	MgO	Na ₂ O	K ₂ O	Fe ₂ O ₃	TiO ₂	LoI
Content (%)	17.4	7.4	12.3	2.1	0.4	0.5	47.7	0.5	5.9
Element	P	Zn	S	Ag					
Content	2.3 (%)	7.1 (%)	2.1 (%)	27.5 (ppm)					

The chemical analysis highlighted the relatively high content of lead (2.3%) and zinc (7.1%). The content of silver was approximately 27 ppm. Application of various separation and beneficiation methods for slag enrichment could increase the content of Pb, Zn, and Ag, which would lead to their further exploitation. The chemical composition analysis indicates that micronized slag could be used as an addition in cement clinker production [37–41] or, alternatively, as a non-reactive filler or coarse aggregate in concrete [42–49]. The slag used as filler might show certain pozzolanic abilities. The presence of sulfur in the Pb–Zn slag sample in the amount of 2.1% took the form of sulfides or sulfates. Sulfur reacted with oxygen from the air at high temperatures (up to 1000 °C), which resulted in the formation of new compounds. This information may be useful in determining the best technological procedure for separating valuable elements in Pb–Zn slag from existing impurities. Nonetheless, this slag can be added to cement and aggregate in a concrete mix because its total sulfur concentration is less than 2.75% [50,51].

The X-ray diffraction analysis of the Pb–Zn slag is illustrated in Figure 5.

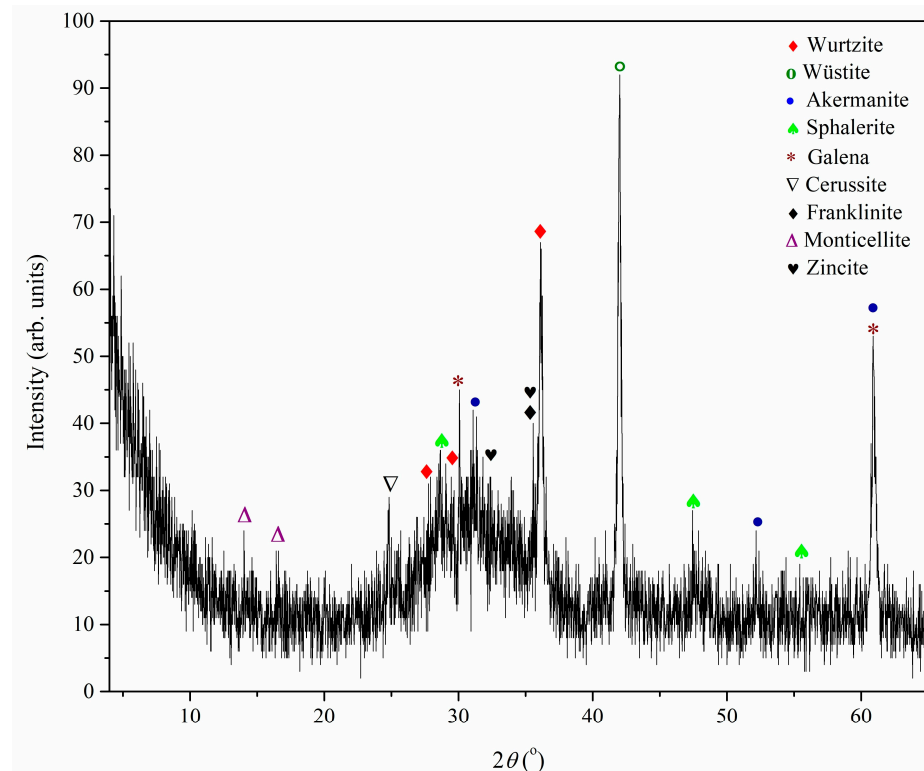


Figure 5. XRD diffractogram of Pb–Zn slag.

The presence of the following crystalline mineral phases was determined in the analyzed sample of Pb–Zn slag: wurtzite ((Zn,Fe)S); sphalerite ($Zn_xFe_{(x-1)}S$, in which x can range from 1 (pure ZnS) to 0.6; galena (PbS); cerussite ($PbCO_3$); akermanite ($(Ca_2Mg[Si_2O_7])$); wüstite (FeO); monticellite ($CaMgSiO_4$); franklinite ($Zn^{2+}Fe_2^{3+}O_4$); and zincite (ZnO). As the Pb–Zn slag sample is a complex multiphase system, some of the mineral phases could not be detected or identified due to the over-lapping or superposing of reflections. The baseline of the XRD diffractogram is elevated, thus the presence of the amorphous phase can be assumed. The amorphous phase is probably related to melted aluminosilicates. Wurtzite is a polymorph of zinc sulfide (Zn,Fe)S, with a hexagonal crystal structure. There is variation in the iron content up to 8%. Wurtzite is typically found as massive, resinous, dark reddish-brown, black to dark reddish-brown, botryoidal banded crusts, and, less frequently, as hemimorphic pyramidal, or tabular, crystals [52,53]. Wurtzite hardness is 3.5–4 on the Mohs scale, which is less than quartz (7 on the Mohs scale of hardness), the main constituent of sand and gravel used for concrete. Iron(II) oxide can be found in the crystalline form wüstite (FeO). In reflected light, this mineral shows grey color with a greenish tinge. Wüstite crystallizes as opaque to translucent metallic grains in the isometric-hexoctahedral crystal structure. Its Mohs hardness ranges from 5 to 5.5. [8,53]. Franklinite ($Zn^{2+}Fe_2^{3+}O_4$) is an oxide mineral that is a member of the iron series of the typical spinel subgroup. Franklinite may include both ferrous (2^+) and ferric (3^+) iron, similar to another spinel component magnetite. Zinc (Zn) is often accompanied by divalent iron and/or manganese (Mn), while trivalent manganese can partially replace ferric iron. Its hardness is 5.5–6 (Mohs scale). Franklinite is associated with a diverse range of minerals, many of which are luminous. This mineral appears as dispersed, microscopic black crystals with octahedral sides that are occasionally visible, but can be, rarely, encountered as a single, large euhedral crystal [8,53]. Monticellite is an olivine group gray silicate mineral ($CaMgSiO_4$). Most monticellites have pure magnesium end members; however, rare ferroan monticellites have between 30 and 75 mol.% iron end members. The hardness monticellite is 5–5.5 (Mohs scale) [8,53]. Zincite, the mineral form of zinc oxide (ZnO), is present at 32° and 36° . Zinc sulfide (ZnS) mineral sphalerite has a bronze-black and honey-yellow hue.

In its pure state, the mineral has 67% zinc metal. It is the most significant zinc ore. The majority of the sizable zinc deposits of the sedimentary exhalative (SEDEX) type are linked to the mineralization of lead, copper, silver, cadmium, nickel, and gold. Sphalerite has relatively low hardness (3.5–4.0 on the Mohs scale) [51,53]. Galena ($\text{Pb}^{2+}\text{S}^{2-}$ or PbS) is a mineral that contains lead sulfide. It is the world's most important lead ore and a significant silver ore. It can be found in skarns, sedimentary rocks, pyrite, chalcopyrite, sphalerite, tennantite–tetrahedrite, and other ore veins. It can also be deposited in pore spaces or can replace carbonate beds in sedimentary rocks. When fresh, the crystals are bright, but exposure to air frequently causes them to tarnish. Galena has a Mohs hardness range of 2.5 to 2.7, making it moderately soft [53,54]. Cerussite (PbCO_3) is a mineral composed of lead carbonate that is typically found in the oxidized zone of lead ore deposits. It has a Mohs hardness of 3 to 3.7. It is a common aging product of galena and other lead ore minerals weathering. The mineral cerussite is interesting because it can form in a variety of crystal formations with odd twinning habits [53–55]. Akermanite, a mineral composed of dicalcium magnesium disilicate, $\text{Ca}_2\text{MgSi}_2\text{O}_7$, is a member of the melilite mineral series. Melilite is a group of sorosilicate minerals made up of calcium silicates of magnesium and aluminum; the magnesian end member is akermanite, and the aluminous end member is gehlenite. These minerals crystallize from a variety of artificial melts, blast-furnace slags, and calcium-rich alkaline magmas. The most common places to find them are in contact zones of thermally metamorphosed limestones and in impure carbonate rocks that have been transformed into feldspathoidal rocks by basic magmas. Akermanite is classified as a 5 or a 6 on the Mohs mineral hardness scale [56,57]. According to the mineral hardness, which is comparatively lower than that of standard aggregate for concrete, during crushing and subsequent milling, mineral materials mostly form the fine aggregate share (i.e., sand or filler), while crushed glassy content will form the coarse aggregate share.

The samples of Pb–Zn slag were observed using optical microscopy on a Carl Zeiss-Jena's JENAPOL-U polarizing microscope (described in Section 2.4). The grain mixtures were distributed on a plexiglass carrier and observed in either transmitted or reflected light. The microphotographs of the samples are provided in Figure 6.

The details visible in the microphotographs of the slag samples are as follows: (a) spherical lead inclusions in a glassy matrix recorded in air and reflected light (marked with green arrow); (b) complex intergrowths of Pb and Zn phases with sphalerite, galena (marked with green arrow) and dark gray inclusions of cerussite (marked with red arrows), both recorded in air and reflected light; (c) complex intergrowths of Pb and Zn phases with sphalerite, galena, and wurtzite recorded in air and reflected light (marked with green arrow); (d) a simple fusion of a intergrowths of various lead phases with a vitreous matrix recorded in air and reflected light (marked with green arrow); (e) a simple fusion of sphalerite and amorphous matter recorded in air and reflected light (marked with green arrow); (f) inclusions of elemental silver (shiny white dots) in the glassy matrix recorded in oil and reflected light (marked with red arrows); (g) an inclusion of elemental copper in the glassy matrix recorded in oil and reflected light (marked with red arrow); (h) inclusions of elemental silver (shiny white dots) in the glassy matrix recorded in oil and reflected light (marked with red arrows); (i) an inclusion of elemental silver (shiny white dot) in the glassy matrix recorded in oil and reflected light (marked with red arrows); (j) inclusions of elemental copper (bright reddish-yellow dots in a glassy matrix recorded in oil and reflected light (marked with green arrows)); (k) oval inclusions of elemental silver (shiny white dots) in lead phase intergrowths recorded in oil and reflected light (marked with red arrows); (l) inclusions of elemental silver (brilliant white) in lead phase intergrowths recorded in oil and reflected light (marked with red arrows); (m) inclusions of elemental copper (bright orange) in a glassy matrix recorded in oil and reflected light (marked with green arrows); and (n) simple fusion of intergrowths of Pb and Zn phases recorded in air and reflected light (marked with green arrow).

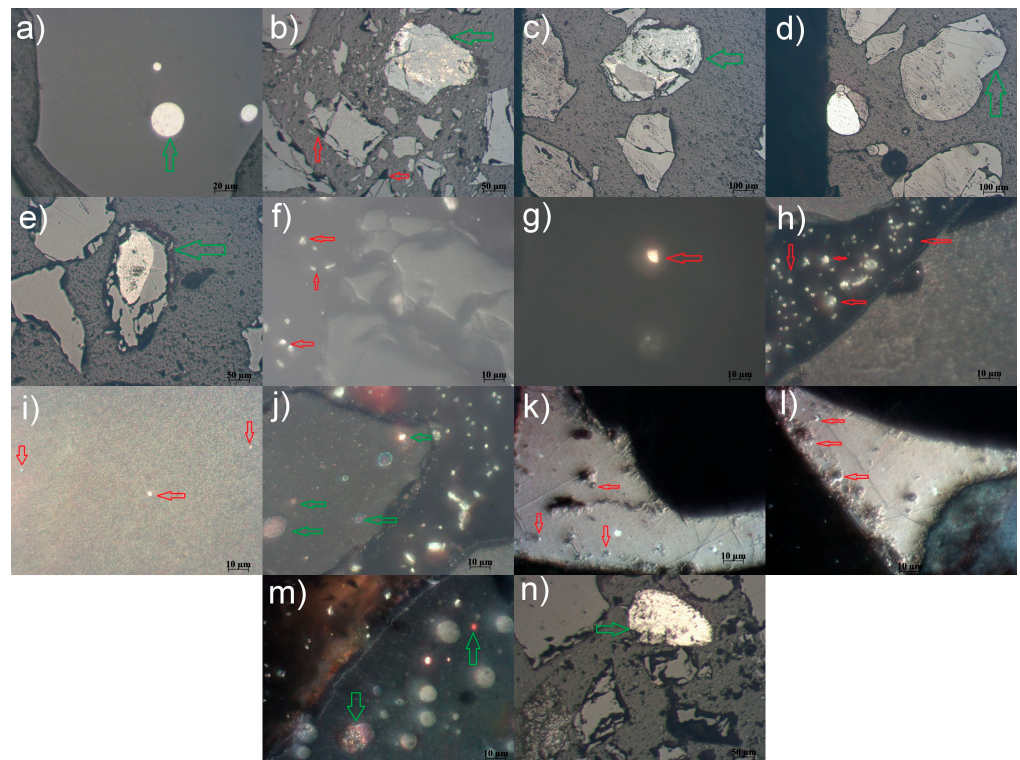


Figure 6. Microphotographs of Pb–Zn slag samples.

Based on the obtained qualitative XRD mineralogical analysis and optical microscopy, the original sample of Pb–Zn slag comprised a complex mixture of the following phases: wurtzite, sphalerite, galena, cerussite, akermanite, wüstite, monticellite, franklinite, and zincite. The presence of an amorphous phase was confirmed by microphotographs. The vitreous matrix is clearly visible in Figure 6d,f–h,j,m. Complex intergrowths of various Pb and Zn phases are predominant in the analyzed samples. Sphalerite and galena, as well as dark gray inclusions of cerussite, are identified in Figure 6b. Wurtzite was present in the sample presented in Figure 6c. Silver immersed in intergrowths of lead phases is also noticed. The amorphous phase (glassy matrix) of aluminosilicates, spinel, silicate, and mixed (spinel–silicate) composition, as previously assumed, is the predominant phase in observed samples. According to chemical analysis, this phase is Al–Si rich, indicating possible pozzolanic characteristics of the slag. Mineral phases (wurtzite, sphalerite, galena, and cerussite) mostly appear as skeletal formations in the glassy matrix. Their abundance can be estimated as relatively low, according to the microstructural preview presented in the microphotographs.

Regarding further refinement procedures and the extraction of Pb and Zn, the assumption is that complex intergrowths of lead and zinc phases can be initially processed by a combination of gravity concentration and separation techniques in order to increase the content of these elements. Similar procedures can be applied to elemental silver and copper, although their content is low. Amorphous aluminosilicate residue obtained upon initial concentration and separation processes can be repurposed and used in the design of building materials such as mortar and concrete. Regardless of how small, this would be a step towards closing a recycling circle and achieving a zero-waste agenda.

A more precise preview of the microstructure of Pb–Zn slag is given in SEM microphotographs (Figure 7). The EDS analysis of the characteristic points and areas is also provided in the SEM images (Figure 7). The EDS elemental analysis is presented in Table 3.

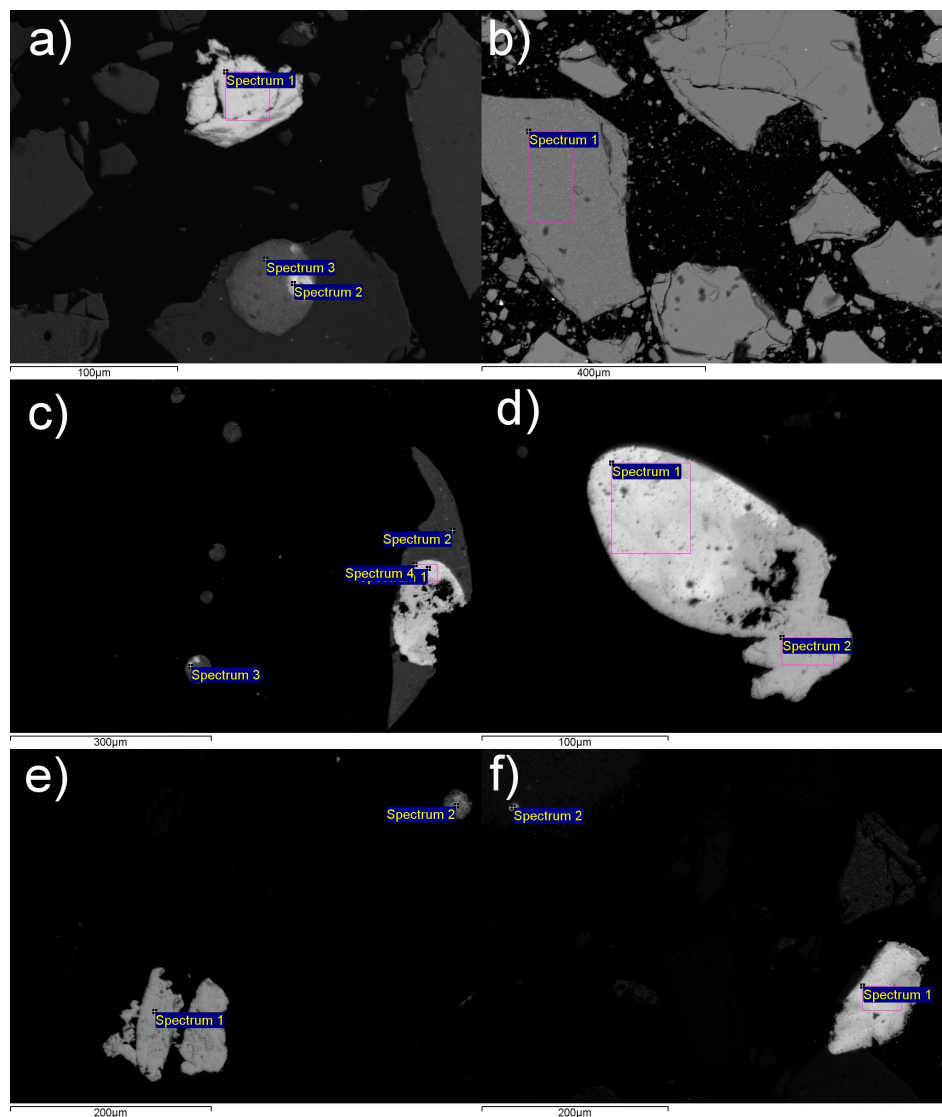


Figure 7. SEM microphotograph of Pb–Zn slag sample.

Table 3. Chemical analyses of selected grains of the Pb–Zn slag sample (EDS method).

Pt *. Figure 7	Pb (%)	Cu (%)	Fe (%)	As (%)	S (%)	O (%)	Fe (%)	Ca (%)	Si (%)	Al (%)	Zn (%)	Ag (%)
7a/1	75.23	0.79	0.70	-	-	22.40	-	-	-	-	-	-
7a/2	55.73	16.77	3.76	1.1	13.30	8.62	-	-	-	-	-	-
7a/3	68.41	0.92	0.60	-	10.24	20.54	-	-	-	-	-	-
7b/1	-	0.60	-	-	-	30.30	29.05	7.03	18.26	12.45	16.67	-
7c/1	82.69	2.36	-	-	-	14.95	-	-	-	-	-	-
7c/2	80.25	1.98	-	-	-	15.98	-	-	-	-	-	-
7c/3	78.74	2.56	-	-	-	16.78	-	-	-	-	-	-
7c/4	79.05	3.50	0.95	-	-	16.50	-	-	-	-	-	-
7d/1	84.62	2.36	-	-	-	13.01	-	-	-	-	-	-
7d/2	76.23	-	-	-	0.54	21.81	-	1.41	-	-	-	-
7e/1	-	-	8.94	-	36.97	8.81	-	2.53	3.56	1.28	33.10	0.91
7e/2	-	-	6.57	-	32.21	9.25	-	1.57	2.89	1.54	38.41	0.74
7f/1	90.70	0.46	-	-	-	7.76	-	-	-	-	-	0.97
7f/2	91.4	0.37	-	-	-	8.54	-	-	-	-	-	0.82

* Point in Figure 7a–f.

SEM analysis combined with EDS elemental mapping revealed that the Pb–Zn slag sample is primarily composed of oxidized complex intergrowths of lead phases, oxidized complex intergrowths of zinc phases, and a vitreous matrix made of amorphous aluminosilicates, amorphous silicates, and mixtures of spinel and silicates. Very small grains are grouped in complex agglomerations or specific formations (Figure 7e). Grains larger than 100 µm in diameter are mostly free or appear as simple formations (Figure 7d). The largest diameters of these phases go up to 300 µm (block-shaped grains in Figure 7b).

A combination of results provided by SEM and EDS analyses point out the presence of various mineral phases and their complex intergrowths in the Pb–Zn sample. A relatively large particle, which corresponds to cerussite, is presented in Figure 7(a-1). EDS analysis identified high Pb content (75.23%) in position 1 on this particle. The Fe and Cu contents are very low; therefore, they might originate from an inclusion combined with a cerussite particle. This inclusion can be correlated with wüstite (FeO). Particles in positions 2 and 3 (Figure 7a) correspond to the mineral galena according to elemental mapping and detection (Table 3). Significant amounts of Pb and S are detected in these particles. Iron might originate from small inclusions of wüstite, especially in the particle 7a-2. There is a certain content of copper present in this sample (7a), as well as in samples 7b-1, 7c1-4, 7d-1, 7f-1, and 7f-2. Copper has not previously been detected by either the AAS (in the form of oxide) or XRD method (in the form of a mineral). It is possible that, though the accuracy and precision of the sampling were maintained at the highest level possible, the chosen grain mixtures used for microscopy (and subsequently for EDS) comprised certain Cu inclusions. The Cu inclusions were recorded by optical microscopy (for instance, Figure 6m), and SEM and EDS confirmed their presence. Copper might be included in complex intergrowths of one or various present mineral phases.

Spectrum 1 in Figure 7b. is characterized by significant contents of O, Ca, Si, Al, and Zn, which can be correlated with zincite primarily, followed by akermanite, or possibly monticellite (or complex intergrowths of these mineral phases). The grains are immersed in a vitreous Al–Si matrix, as can be seen in Figure 7b. Spectra 1, 2, 3, and 4 in Figure 7c. are correlated with high Pb content (82.69%, 80.25%, 78.74%, and 79.05%, respectively), which means that the observed particles belong to the mineral cerussite. Particle 7c-4 contains iron; thereby, it can be correlated with a possible small quantity of the mineral wüstite. Particle 7d-1 probably corresponds to cerussite (PbCO₃), while particle 7d-2 might be cerussite or galena, followed by the inclusion of akermanite or monticellite (Ca = 1.41%).

Figure 7e illustrates two particles—one larger and more complex, the other significantly smaller. Both particles 7e-1 and 7e-2 comprise relatively high Zn content (33.10% and 38.41%, respectively), S content (36.97% and 32.21%, respectively), and certain quantities of Fe (8.94% and 6.57%, respectively). These particles might correspond to wurtzite or sphalerite (Zn–Fe–S combination), or zincite (ZnO). The presence of low calcium amounts refers to the possible occurrence of akermanite or monticellite in traces. The EDS quantification of spectra in Figure 7(f-1,f-2) shows the predominant presence of Pb, thereby indicating that the observed particles probably correspond to cerussite. Small quantities of elemental silver were detected in particles recorded in Figure 7e,f. Silver particles are usually oval-shaped, but elemental silver can also be found in the form of tiny wires with lengths of up to 5 µm. Aside from this, elemental silver and copper occur as small inclusions in the glassy matrix or complex mineral intergrowths, rarely exceeding 2–3 µm (silver) and 7–8 µm (copper). Additionally, elemental silver is frequently found in host grain cracks [8,52,53].

A plan for the next stage of the experiment is to try to condense the metals into a collective concentrate from which the biggest quantity of lead, zinc, and silver might be extracted. These tests should be carried out using a combination of gravity concentration and separation techniques to detach metal concentrates from the glassy matrix.

Application of Pb–Zn Slag in Construction Materials

Waste materials from metallurgy have to be repurposed and utilized more regularly in order for the current linear economy to make the transition to a more circular economy.

This has resulted in numerous examples of these materials being reapplied as mineral additives or aggregates in various building materials, including cement, mortars, concrete, masonry bricks, and geopolymers [20–26]. The analyzed Pb–Zn slag’s high concentration of aluminosilicate amorphous phase is a good sign that this material could be used for producing building composites. An experimental material must meet specific requirements for standard building materials before it can be used in the construction industry (e.g., EN standards or their national versions are often applied). Therefore, initial testing is carried out on the production of cement mortars with Pb–Zn slag addition.

For the experiment, four cement mortars were prepared. The bonding agent that was employed in all mortars is ordinary Portland cement (OPC), CEM I 42.5R, Lafarge. Its specific surface area is 292 m²/kg. The CEM–N mortar was used for comparison of the results. High-purity quartz sand (SiO₂ = 98.1%; uncompact bulk density 1640 kg/m³, and compacted bulk density 1750 kg/m³) was utilized as aggregate in the CEM–N sample. The grain size distribution of quartz aggregate was as follows: 0.063–0.5 mm = 30%, 0.5–1.0 mm = 40%, 1.0–2.0 mm = 20%, and 2.0–4.0 mm = 10%.

Pulverized Pb–Zn slag was used as a mineral additive in the CEM–PbZn10, CEM–PbZn20, and CEM–PbZn30 experimental mortars. Slag is employed both as filler (due to its small average grain diameter, i.e., d₅₀ = 10 μm) and as cement replacement (due to its vitreous Al–Si origin). Crushed Pb–Zn slag (grain sizes 0.063–4.0 mm) was used as aggregate. The grain size distribution of the slag-made aggregate was: 0.063–0.5 mm = 30%, 0.5–1.0 mm = 40%, 1.0–2.0 mm = 20%, and 2.0–4.0 mm = 10%.

The chemical composition of the cement was determined using the AAS technique and is as follows (the method was described in Section 2.4): SiO₂ = 21.95%; Al₂O₃ = 5.41%; Fe₂O₃ = 3.05%; CaO = 61.98%; MgO = 2.69%; K₂O = 0.91%; Na₂O = 0.10%; TiO₂ < 0.1%; SO₃ = 2.15%; loss on ignition at 1000 °C = 0.96%. Chemical composition of Pb–Zn slag is provided in Table 2.

The mix design of the experimental mortars is provided in Table 4.

Table 4. Mix design of the experimental mortars.

Sample	OPC (%)	Pb–Zn Slag— Coarse Fraction (%)	Pb–Zn Slag— Pulverized (%)	Natural Aggregate— Quartz Sand (%)
CEM–N	40	-	-	60
CEM–PbZn10	36	60	4	-
CEM–PbZn20	32	60	8	-
CEM–PbZn30	28	60	12	-

Mortar samples were prepared using the standard procedure [58] according to the mix design shown in Table 4. Using a laboratory mixer, cement, aggregate, and filler were initially dry homogenized. Water was added later in the mixing process. Fresh mortar was placed in steel molds (40 × 40 × 160 mm) and stored for one day in a climate chamber (95 ± 5% relative humidity and 20 °C (+3 °C/−2 °C)). Upon removal from the molds, samples were stored in the climate chamber under the same conditions for a total of 7 days. Following that, the samples were cured for 21 days at 65 ± 5% relative humidity. The rheology of the fresh mortar was determined via a slump test using a flow table [59]. Bulk density of fresh mortar and dry bulk density of hardened mortar [60,61], determination of water absorption coefficient due to capillary action of hardened mortar [62], and compressive and flexural strengths [63] were determined using standard methods. All obtained testing results represent an average of at least three tests.

Experimentally determined physico-mechanical properties of fresh and hardened mortar samples (workability of fresh mortar in mm; bulk density of fresh mortar in kg/m³; bulk density of hardened mortar in kg/m³; and water absorption coefficient in mg/m²·min^{0.5}) are illustrated in graphs provided in Figure 8.

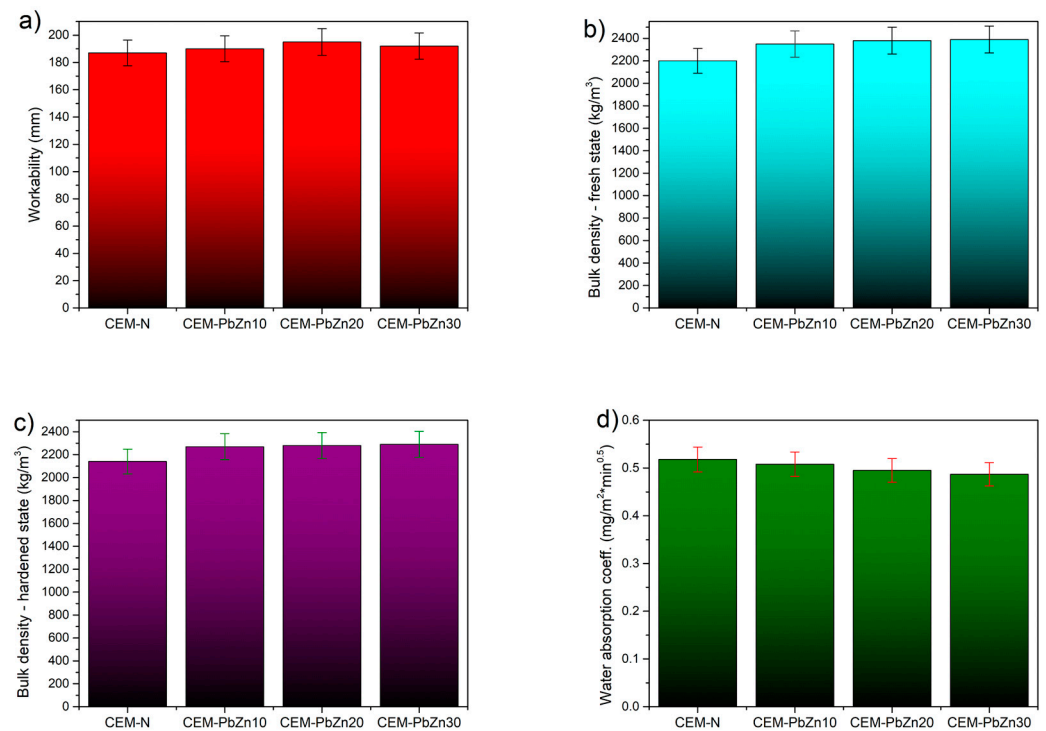


Figure 8. Physico-mechanical properties of mortar samples: (a) workability, (b) bulk density of fresh mortar, (c) bulk density of hardened mortar, and (d) water absorption coefficient.

In comparison with standard cement mortar, the workability of experimental mortar samples increased with the addition of Pb–Zn slag filler (the workability of the CEM–N sample was 187 mm). CEM–PbZn20 has the highest workability value (195 mm), indicating that adding more than 20% filler has a negative impact on the physico-mechanical properties of mortars in their fresh state. Bulk density, measured both in fresh and hardened states, showed an increasing trend. CEM–PbZn10, CEM–PbZn20, and CEM–PbZn30 samples had higher bulk density values than CEM–N (2200 kg/m³ and 2140 kg/m³ in fresh and hardened states, respectively). Because of the difference in specific gravities of aggregates, the bulk densities in the fresh state of mortars with slag are 150, 180, and 190 kg/m³ higher for the CEM–PbZn10, CEM–PbZn20, and CEM–PbZn30 samples, respectively. Namely, the specific gravity of Pb–Zn slag varies between 2500 and 3600 kg/m³ [64], while the specific gravity of silica sand is usually 1730–1750 kg/m³ [65]. The differences between bulk densities in the hardened state were similar: 130, 140, and 150 kg/m³ for the CEM–PbZn10, CEM–PbZn20, and CEM–PbZn30 samples, respectively. The addition of fine Pb–Zn slag, as well as the substitution of standard aggregate with coarse Pb–Zn slag aggregate, influenced the increase in bulk densities. Pb–Zn mortar samples had lower water absorption coefficients than standard mortar (CEM–N). The values of the water absorption coefficient decrease with increasing content of Pb–Zn filler. The addition of filler aided in the better ‘packing’ of the microstructure, leaving fewer voids and pores behind, and thus lowering the examined material’s water absorption capability [66,67].

Values of mechanical strengths (CS—compressive strength and FS—flexural strength) measured after 2, 7, and 28 days of hardening are illustrated in Figure 9.

As shown in Figure 9a, differences in initial compressive strengths were more pronounced during the early stages of mortar hardening. After two days of hardening, the compressive strength of the CEM–PbZn10 sample was 25% higher than the CS-2 of the standard mortar sample (CEM–N). There was a 35.6% difference in CS-2 between CEM–PbZn20 and CEM–N, and a 30% difference between CEM–PbZn30 and CEM–N. For CEM–PbZn10, CEM–PbZn20, CEM–PbZn30, and CEM–N, the differences in the final 28-day strengths (CS-28) were 14.14%, 23.8%, and 17.9%, respectively. A higher increase in initial strengths can be explained by the pozzolanic effect of Pb–Zn slag filler [68]. The CEM–PbZn20

sample has the highest final compressive strength (CS-28 = 53.05 MPa), indicating that the Pb–Zn filler contributes the most in its quantity of 20%. Therefore, it can be seen that a slag-based filler content of over 20% has no beneficial effect on mechanical strengths.

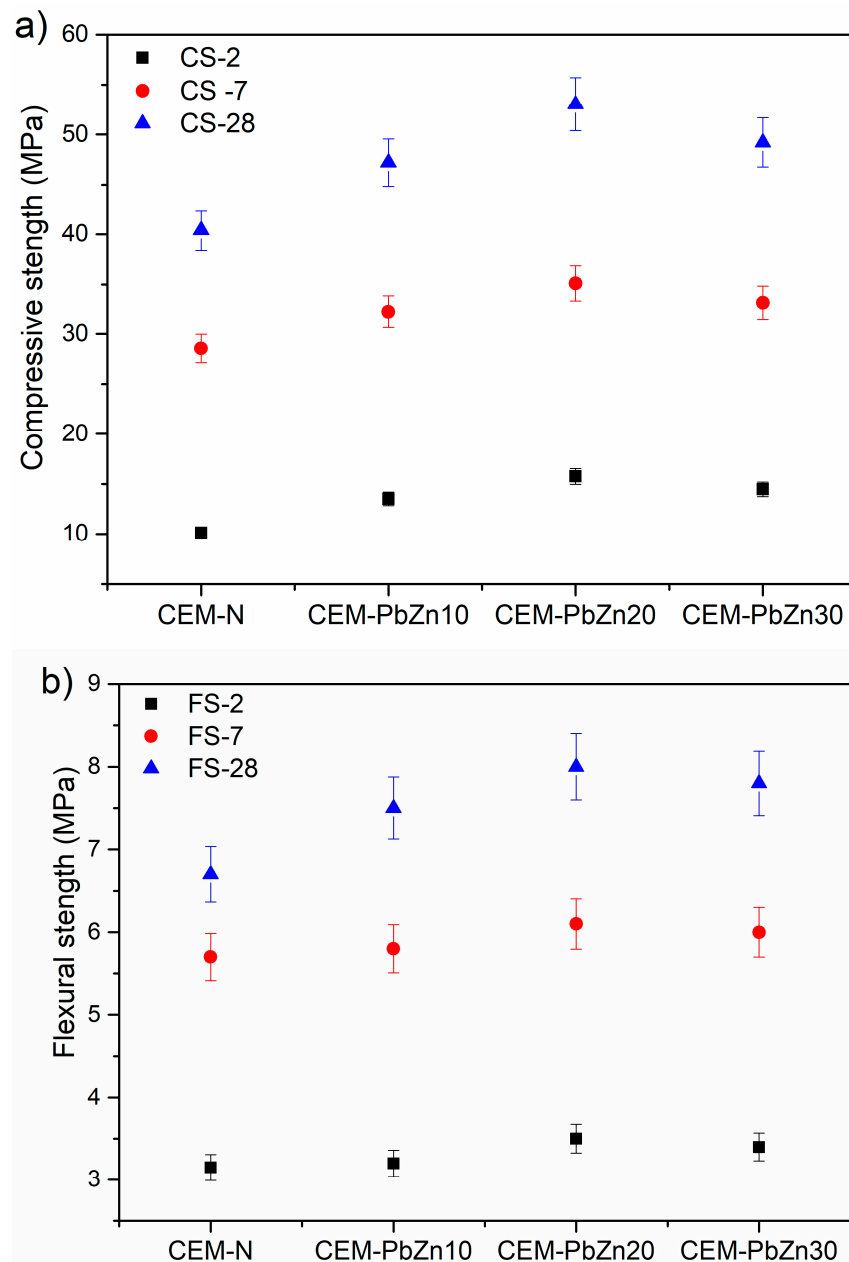


Figure 9. Mechanical strengths of mortars. (a) Compressive strengths and (b) flexural strengths.

Flexural strengths (Figure 9b) show a similar distribution of strengths in the diagram. Namely, the CEM–PbZn20 sample yielded the highest values for FS-2 and FS-28 (3.5 and 8 MPa, respectively). The differences in initial flexural strengths of slag-based mortars and cement mortars were 2%, 10%, and 8% for CEM–PbZn10, CEM–PbZn20, and CEM–PnZn30, respectively. The final flexural strengths (FS-28) differed from CEM–N by 11%, 16%, and 15%, respectively.

4. Conclusions

The historic Pb–Zn slag from the smelter plant (Topilnica, Veles, North Macedonia) was characterized based on physico-chemical, mineralogical, and microstructural properties in order to propose its potential reapplications. The obtained results will serve as the

foundation for more extensive technological tests that will define the procedures for refining Pb–Zn slag and separating valuable metals (such as lead, zinc, and silver) and will help optimize the procedure for manufacturing commercial building products, with the ultimate goal of closing the slag’s life cycle in accordance with circular economy and zero waste principles. The main conclusions are summarized below:

- The possibility of further refinement and extracting valuable metals is considered due to a certain content of lead (2.3%), zinc (7.1%), and silver (27 ppm), identified in the investigated waste material by atomic absorption spectroscopy.
- Optical microscopy and scanning electron microscope analyses revealed certain contents of metallic droplets (lead, zinc, silver, and copper) in the Pb–Zn slag. X-ray diffraction analysis supported the previous finding by detecting the crystalline mineral phases wurtzite, sphalerite, galena, cerussite, akermanite, wüstite, monticellite, franklinite, and zincite. In theory, the concentration of metal elements (Pb, Zn, Ag, and Cu) in slag might be increased upon application of gravity concentration and separation techniques for dividing metallic crystalline phases from the amorphous Al–Si matrix. This would be an initial step in further refining slag using a pyrometallurgical or hydrometallurgical process to recover the metals in question. The economic viability of the proposed process remains to be determined, but as waste material is used, the proposed method might be a step towards closing the gap in the recycling and reapplication of waste circle and achieving a number of sustainable development goals.
- The presence of the alumino-silicate amorphous phase in Pb–Zn slag samples is important for the reapplication of this alternative raw material in the building sector. Namely, the amorphous alumino-silicates and silicates, as well as mixed spinel–silicate phases of slag, with high concentrations of SiO₂, Al₂O₃, CaO, and Fe₂O₃, are suitable for producing the mineral additives used as partial cement replacement, fillers, and coarse aggregate for concrete or mortar.
- The study revealed that producing composite waste-based mortars with 20% of pulverized Pb–Zn slag as an optimal cement replacement and slag-based aggregate is feasible. Namely, the experimental CEM–PbZn20 mortar demonstrated a final 28-day strength that was 23.8% higher than that of standard cement mortar. The high strength of slag-based mortar was induced by a combination of the pozzolanic behavior of pulverized Pb–Zn slag.
- Based on the composition and microstructure of the slag, it can be assumed that this metallurgical waste can be further refined and reused. In terms of circular economy principles, Pb–Zn slag has a high re-utilization potential, so it was critical to thoroughly investigate the material and establish methods of concentrating useful components and processing them into commercial products.

Author Contributions: Conceptualization, D.R., A.T. and J.S.; methodology, D.R., A.T. and J.S.; validation, D.R., A.T. and J.S.; formal analysis, D.R., J.S., V.J., D.T. and B.I.; investigation, D.R., A.T. and J.S.; writing—original draft preparation, review and corrections, A.T., D.R. and J.S.; supervision, A.T. All authors have read and agreed to the published version of the manuscript.

Funding: This research was funded by the Ministry of Science, Technological Development and Innovation of the Republic of Serbia (Contract No.: 451-03-47/2023-01/200012 and 451-03-47/2023-01/200023) and Project: 101111694—GREENCO—ERASMUS-EDU-2022-PI-ALL-INNO.

Institutional Review Board Statement: Not applicable.

Informed Consent Statement: Not applicable.

Data Availability Statement: Data are contained within the article.

Conflicts of Interest: The authors declare they have no competing interest or financial conflict among them.

References

1. Chen, D.T.; Roy, A.; Li, Y.; Bogush, A.; Au, W.Y.; Stegemann, J. Speciation of toxic pollutants in Pb/Zn smelter slags by X-ray Absorption Spectroscopy in the context of the literature. *J. Hazard. Mater.* **2023**, *460*, 132373. [CrossRef] [PubMed]
2. Available online: www.statista.com (accessed on 21 December 2023).
3. Kania, H.; Saturnus, M. Evaluation and Current State of Primary and Secondary Zinc Production—A Review. *Appl. Sci.* **2023**, *13*, 2003. [CrossRef]
4. Available online: <https://www.teck.com/media/Carbon-Footprint-of-Teck-Special-High-Grade-Zinc.pdf> (accessed on 21 December 2023).
5. Bača, P.; Vanýsek, P. Issues Concerning Manufacture and Recycling of Lead. *Energies* **2023**, *16*, 4468. [CrossRef]
6. EPA. Available online: <https://www.epa.gov> (accessed on 21 December 2023).
7. Buch, A.C.; Niemeyer, J.C.; Marques, E.D.; Silva-Filho, E.V. Ecological risk assessment of trace metals in soils affected by mine tailings. *J. Hazard. Mater.* **2021**, *403*, 123852. [CrossRef]
8. Nowińska, K.; Zdzisław, A. Slags of the Imperial Smelting Process for Zn and Pb Production. In *Reference Module in Materials Science and Materials Engineering*; Hashmi, S., Ed.; Elsevier: Oxford, UK, 2017; pp. 1–5, ISBN 978-0-12-803581-8. [CrossRef]
9. Sun, Z.; Hu, Y.; Cheng, H. Public health risk of toxic metal(loid) pollution to the population living near an abandoned small-scale polymetallic mine. *Sci. Total Environ.* **2020**, *718*, 137434. [CrossRef]
10. Safa, M.; Goodarzi, A.; Lorestani, B. Enhanced post freeze-thaw stability of Zn/Pb co-contaminated soil through MgO-activated steel slag and fiber treatment. *Cold Reg. Sci. Technol.* **2023**, *210*, 103826. [CrossRef]
11. Ettler, V.; Johan, Z. 12 years of leaching of contaminants from Pb smelter slags: Geochemical/mineralogical controls and slag recycling potential. *Appl. Geochem.* **2014**, *40*, 97–103. [CrossRef]
12. Wang, W.; Gan, Y.; Kang, X. Synthesis and characterization of sustainable ecofriendly unburned bricks from slate tailings. *J. Mater. Res. Technol.* **2021**, *14*, 1697–1708. [CrossRef]
13. Wang, P.; Li, J.; Hu, Y.; Cheng, H. Solidification and stabilization of Pb–Zn mine tailing with municipal solid waste incineration fly ash and ground granulated blast-furnace slag for unfired brick fabrication. *Environ. Pollut.* **2023**, *321*, 121135. [CrossRef]
14. Han, L.-J.; Li, J.-S.; Xue, Q.; Guo, M.-Z.; Wang, P.; Poon, C.S. Enzymatically induced phosphate precipitation (EIPP) for stabilization/solidification (S/S) treatment of heavy metal tailings. *Constr. Build. Mater.* **2022**, *314*, 125577. [CrossRef]
15. Fawzy, M.; El Ghar, S.; Gaafar, I.; El Shafey, A.; Diab, M.; Hussein, A. Recovery of valuable heavy minerals via gravity and magnetic separation operations from Diit Quaternary stream sediments, southern coast of the Red Sea, Egypt. *J. Phys. Conf. Ser.* **2022**, *2305*, 012020. [CrossRef]
16. Huston, D.L.; Stevens, B.; Southgate, P.N.; Muhling, P.; Wyborn, L. Australian Zn-Pb-Ag Ore-Forming Systems: A Review and Analysis. *Econ. Geol.* **2006**, *101*, 1117–1157. [CrossRef]
17. Alzhanova, G.Z.; Aibuldinov, Y.K.; Iskakova, Z.B.; Khabidolda, S.M.; Abdiyussupov, G.G.; Omirzak, M.T.; Murali, G.; Vatin, N.I. Development of Environmentally Clean Construction Materials Using Industrial Waste. *Materials* **2022**, *15*, 5726. [CrossRef] [PubMed]
18. Monteiro, N.B.R.; da Silva, E.A.; Moita Neto, J.M. Sustainable development goals in mining. *J. Clean. Prod.* **2019**, *228*, 509–520. [CrossRef]
19. UN Foundation. Available online: <https://unfoundation.org/what-we-do/issues/sustainable-development-goals/> (accessed on 21 December 2023).
20. Kanneboina, Y.; Saravanan, J.; Kabeer, T.; Bisht, K. Valorization of lead and zinc slags for the production of construction materials—A review for future research direction. *Constr. Build. Mater.* **2023**, *367*, 130314. [CrossRef]
21. Anandaraj, S.; Karthik, S.; Vijaymohan, S.; Rampradheep, G.; Indhiradevi, P.; Anusha, G. Effects of using white flour, zinc oxide and zinc ash as an admixture in mortar and concrete. *Mater. Today Proc.* **2022**, *52*, 1788–1793. [CrossRef]
22. Xu, L.; Sun, Z.; Tang, C.; Yang, K.; Li, B.; Zhang, Y.; Yang, Z.; Wu, K. Mitigation effect of accelerators on the lead–zinc tailing induced retardation in autoclaved concrete. *Constr. Build. Mater.* **2022**, *352*, 128929. [CrossRef]
23. Wang, H.; Ju, C.; Zhou, M.; Zheng, F.; Dong, Y.; Hou, H.; Liu, S. Grinding kinetics of lead–zinc tailing powders and its optimal particle size as a pozzolanic admixture in cement mortar. *Adv. Powder Technol.* **2022**, *33*, 103730. [CrossRef]
24. Murmu, A.L.; Patel, A. Towards sustainable bricks production: An overview. *Constr. Build. Mater.* **2018**, *165*, 112–125. [CrossRef]
25. Chen, Y.; Zhang, Y.; Chen, T.; Zhao, Y.; Bao, S. Preparation of eco-friendly construction bricks from hematite tailings. *Constr. Build. Mater.* **2011**, *25*, 2107–2111. [CrossRef]
26. Zhao, Y.; Zhang, Y.; Chen, T.; Chen, Y.; Bao, S. Preparation of high strength autoclaved bricks from hematite tailings. *Constr. Build. Mater.* **2012**, *28*, 450–455. [CrossRef]
27. Zhang, X.; Li, L.; Ul Hassan, Q.; Pan, D.; Zhu, G. Preparation and characterization of glass ceramics synthesized from lead slag and lead-zinc tailings. *Ceram. Intern.* **2023**, *49*, 16164–16173. [CrossRef]
28. Li, J.; Liu, Y.; Ke, X.; Jiao, X.; Li, R.; Shi, C. Geopolymer synthesized from electrolytic manganese residue and lead-zinc smelting slag: Compressive strength and heavy metal immobilization. *Cem. Concr. Comp.* **2022**, *134*, 104806. [CrossRef]
29. Morrison, C.; Hooper, R.; Lardner, K. The use of ferro-silicate slag from ISF zinc production as a sand replacement in concrete. *Cem. Concr. Res.* **2003**, *33*, 2085–2089. [CrossRef]
30. Atzeni, C.; Massida, L.; Sanna, U. Use of Granulated Slag from Lead and Zinc Processing in Concrete Technology. *Cem. Concr. Res.* **1996**, *26*, 1381–1388. [CrossRef]

31. Buzatu, T.; Talpos, E.; Petrescu, M.; Ghica, V.; Iacob, G.; Buzatu, M. Utilization of granulated lead slag as a structural material in roads constructions. *J. Mater. Cycles Waste Manag.* **2015**, *17*, 707–717. [[CrossRef](#)]
32. Prasad, P.S.; Ramana, G.V. Imperial smelting furnace (zinc) slag as a structural fill in reinforced soil structures. *Geotext. Geomembranes* **2016**, *44*, 406–428. [[CrossRef](#)]
33. Mandin, D.; van der Sloot, H.A.; Gervais, C.; Barna, R.; Mehu, J. Valorization of leadzincprimary smelters slags. *Stud. Environ. Sci.* **1997**, *71*, 617–630. [[CrossRef](#)]
34. Duan, X.; Li, X.; Li, Y.; Qi, X.; Li, G.; Lu, Z.; Yang, N. Separation and stabilization of arsenic in copper smelting wastewater by zinc slag. *J. Clean. Prod.* **2021**, *312*, 127797. [[CrossRef](#)]
35. Saedi, A.; Jamshidi-Zanjani, A.; Darban, A.K.; Mohseni, M.; Nejati, H. Utilization of lead–zinc mine tailings as cement substitutes in concrete construction: Effect of sulfide content, *J. Build. Eng.* **2022**, *57*, 104865. [[CrossRef](#)]
36. Chen, W.; Peng, R.; Straub, C.; Yuan, B. Promoting the performance of one-part alkali-activated slag using fine lead-zinc mine tailings. *Constr. Build. Mater.* **2020**, *236*, 117745. [[CrossRef](#)]
37. Doussang, L.; Samson, G.; Deby, F.; Huet, B.; Guillon, E.; Cyr, M. Durability parameters of three low-carbon concretes (low clinker, alkali-activated slag and supersulfated cement). *Constr. Build. Mater.* **2023**, *407*, 133511. [[CrossRef](#)]
38. Turkoglu, M.; Bayraktar, O.Y.; Benli, A.; Kaplan, G. Effect of cement clinker type, curing regime and activator dosage on the performance of one-part alkali-activated hybrid slag/clinker composites. *J. Build. Eng.* **2023**, *68*, 106164. [[CrossRef](#)]
39. Gao, T.; Dai, T.; Shen, L.; Jiang, L. Benefits of using steel slag in cement clinker production for environmental conservation and economic revenue generation. *J. Clean. Prod.* **2021**, *282*, 124538. [[CrossRef](#)]
40. Cao, L.; Shen, W.; Huang, J.; Yang, Y.; Zhang, D.; Huang, X.; Lv, Z.; Ji, X. Process to utilize crushed steel slag in cement industry directly: Multi-phased clinker sintering technology. *J. Clean. Prod.* **2019**, *217*, 520–529. [[CrossRef](#)]
41. Erdoğan, S.; Koçak, T. Influence of slag fineness on the strength and heat evolution of multiple-clinker blended cements. *Constr. Build. Mater.* **2017**, *155*, 800–810. [[CrossRef](#)]
42. Nemade, P.; Pasla, D.; Chandrappa, A. Durability assessment of concrete with natural and Linz Donawitz slag as coarse aggregates. *Constr. Build. Mater.* **2023**, *400*, 132617. [[CrossRef](#)]
43. Ramakrishna, J.; Gopi, R. Experimental investigation on partial replacement of cement and coarse aggregate by rice husk ash and steel slag in concrete. *Mater. Today Proc.* **2023**. [[CrossRef](#)]
44. Chen, Z.; Huang, L.; Yan, L.; Cai, H.; Luo, X.; Li, Y. Autoclaved steel slag coarse aggregate: A potential solution for sustainable concrete production. *Constr. Build. Mater.* **2023**, *400*, 132627. [[CrossRef](#)]
45. Teymouri, E.; Wong, K.S.; Tan, Y.; Pauzi, N. Mechanical behaviour of adsorbent pervious concrete using iron slag and zeolite as coarse aggregates. *Constr. Build. Mater.* **2023**, *388*, 131720. [[CrossRef](#)]
46. Lai, M.H.; Chen, Z.H.; Wang, Y.H.; Ho, J.C.M. Effect of fillers on the mechanical properties and durability of steel slag concrete. *Constr. Build. Mater.* **2022**, *335*, 127495. [[CrossRef](#)]
47. Ballari, S.O.; Raffikbasha, M.; Shirgire, A.; Thakur, L.S.; Thenmozhi, S.; Kumar, B. Replacement of coarse aggregates by industrial slag. *Mater. Today Proc.* **2023**. [[CrossRef](#)]
48. Singh, P.; Roy, A.B.D.; Singh, H. Mechanical and durability properties of concrete incorporating weathered coarse Linz-Donawitz (LD) steel slag. *J. Build. Eng.* **2022**, *61*, 105301. [[CrossRef](#)]
49. Sosa, I.; Thomas, C.; Polanco, I.A.; Setién, J.; Sainz-Aja, J.A.; Tamayo, P. Durability of high-performance self-compacted concrete using electric arc furnace slag aggregate and cupola slag powder. *Cem. Concr. Compos.* **2022**, *127*, 104399. [[CrossRef](#)]
50. Zheng, S.; Lu, X.; Zhao, J.; He, R.; Chen, H.; Geng, Y. Influence of industrial by-product sulfur powder on properties of cement-based composites for sustainable infrastructures. *Constr. Build. Mater.* **2023**, *367*, 130171. [[CrossRef](#)]
51. Huang, S.; Pi, Z.; Cai, C.; Li, H. Utilization of high-sulfur iron ore tailings in cement mortar by considering the influence of curing temperature and tailing content. *J. Build. Eng.* **2023**, *74*, 106826. [[CrossRef](#)]
52. Galsin, J.S. (Ed.) Chapter 1—Crystal Structure of Solids. In *Solid State Physics*; Academic Press: Cambridge, MA, USA, 2019; pp. 1–36, ISBN 9780128171035. [[CrossRef](#)]
53. Mindat. Available online: www.mindat.org (accessed on 21 December 2023).
54. Haldar, S.K. (Ed.) Chapter 1—Minerals and rocks. In *Introduction to Mineralogy and Petrology*, 2nd ed.; Elsevier: Amsterdam, The Netherlands, 2020; pp. 1–51, ISBN 9780128205853. [[CrossRef](#)]
55. Sánchez-Navas, A.; López-Cruz, O.; Vellilla, N.; Vidal, I. Crystal growth of lead carbonates: Influence of the medium and relationship between structure and habit. *J. Cryst. Growth* **2013**, *376*, 1–10. [[CrossRef](#)]
56. Britannica. Available online: www.britannica.com (accessed on 21 December 2023).
57. Pracejus, B. (Ed.) IV/C—Oxides with Metal: Oxygen = 2:3 (M₂O₃ and related compounds). In *The Ore Minerals Under the Microscope*, 2nd ed.; Elsevier: Amsterdam, The Netherlands, 2014; pp. 738–789, ISBN 9780444627254. [[CrossRef](#)]
58. SRPS EN 1015-2:2008; Methods of Test for Mortar for Masonry—Part 2: Bulk Sampling of Mortars and Preparation of Test Mortars. CEN: Bruxelles, Belgium, 2008.
59. SRPS EN 1015-3:2008; Methods of Test for Mortar for Masonry—Part 3: Determination of Consistence of Fresh Mortar (by Flow Table). CEN: Bruxelles, Belgium, 2008.
60. SRPS EN 1015-6:2008; Methods of Test for Mortar for Masonry—Part 6: Determination of Bulk Density of Fresh Mortar. CEN: Bruxelles, Belgium, 2008.

61. SRPS EN 1015-10:2008/A1:2008; Methods of Test for Mortar for Masonry—Part 10: Determination of Dry Bulk Density of Hardened Mortar. CEN: Bruxelles, Belgium, 2008.
62. SRPS EN 1015-18:2008; Methods of Test for Mortar for Masonry—Part 18: Determination of Water Absorption Coefficient Due to Capillary Action of Hardened Mortar. CEN: Bruxelles, Belgium, 2008.
63. SRPS EN 1015-11:2019; Methods of Test for Mortar for Masonry—Part 11: Determination of Flexural and Compressive Strength of Hardened Mortar. CEN: Bruxelles, Belgium, 2019.
64. Wang, G.C. (Ed.) 3—Nonferrous metal extraction and nonferrous slags. In *The Utilization of Slag in Civil Infrastructure Construction*; Woodhead Publishing: Sawston, UK, 2016; pp. 35–61, ISBN 9780081009949. [[CrossRef](#)]
65. Malathy, R.; Rajagopal Sentilkumar, S.R.; Prakash, A.R.; Das, B.B.; Chung, I.-M.; Kim, S.-H.; Prabakaran, M. Use of Industrial Silica Sand as a Fine Aggregate in Concrete—An Explorative Study. *Buildings* **2022**, *12*, 1273. [[CrossRef](#)]
66. Terzić, A.; Radulović, D.; Pezo, M.; Stojanović, J.; Pezo, L.; Radojević, Z.; Andrić, L. Prediction model based on artificial neural network for pyrophyllite mechano-chemical activation as an integral step in production of cement binders. *Constr. Build. Mater.* **2020**, *258*, 119721. [[CrossRef](#)]
67. Hatungimana, D.; Taşköprü, C.; İçhedef, M.; Saç, M.M.; Yazıcı, S. Compressive strength, water absorption, water sorptivity and surface radon exhalation rate of silica fume and fly ash-based mortar. *J. Build. Eng.* **2019**, *23*, 369–376. [[CrossRef](#)]
68. Wang, H.; Ju, C.; Zhou, M.; Chen, J.; Dong, Y.; Hou, H. Sustainable and efficient stabilization/solidification of Pb, Cr, and Cd in lead-zinc tailings by using highly reactive pozzolanic solid waste. *J. Environ. Manag.* **2022**, *306*, 114473. [[CrossRef](#)] [[PubMed](#)]

Disclaimer/Publisher’s Note: The statements, opinions and data contained in all publications are solely those of the individual author(s) and contributor(s) and not of MDPI and/or the editor(s). MDPI and/or the editor(s) disclaim responsibility for any injury to people or property resulting from any ideas, methods, instructions or products referred to in the content.